Vincenzo Aquilanti, Simonetta Cavalli, Dario De Fazio, Alessandro Volpi, Antonio Aguilar, Xavier Giménez, and José Mariá Lucas

---

Articles you may be interested in

Spin-orbit corrected full-dimensional potential energy surfaces for the two lowest-lying electronic states of FH2O and dynamics for the F + H2O → HF + OH reaction
J. Chem. Phys. **138**, 074309 (2013); 10.1063/1.4791640

Evidence for excited spin-orbit state reaction dynamics in F + H 2 : Theory and experiment
J. Chem. Phys. **128**, 084313 (2008); 10.1063/1.2831412

Direct evaluation of the lifetime matrix by the hyperquantization algorithm: Narrow resonances in the F + H 2 reaction dynamics and their splitting for nonzero angular momentum
J. Chem. Phys. **123**, 054314 (2005); 10.1063/1.1988311

Energy-dependent cross sections and nonadiabatic reaction dynamics in F (2 P 3/2 , 2 P 1/2)+n– H 2 →HF (v,J)+ H
J. Chem. Phys. **111**, 8404 (1999); 10.1063/1.480182

Spin–orbit effects in quantum mechanical rate constant calculations for the F+H 2 →HF+H reaction
J. Chem. Phys. **111**, 4013 (1999); 10.1063/1.479703

Hyperquantization algorithm. II. Implementation for the F+H₂ reaction dynamics including open-shell and spin-orbit interactions

Vincenzo Aquilanti,[a] Simonetta Cavalli, Dario De Fazio, and Alessandro Volpi
Dipartimento di Chimica, Università di Perugia, 06123 Perugia, Italy

Antonio Aguilar, Xavier Giménez, and José Mariá Lucas
Departament de Química Física, Universitat de Barcelona, 08028 Barcelona, Spain

This work focuses on numerical aspects and performances of the hyperquantization algorithm, presented in the preceding paper, for a prototypical atom–diatom reaction. Here we provide also the extensions which allow the treatment of excited electronic surfaces. Test calculations have been carried out on the reaction F+H₂ at a total nuclear angular momentum equal to zero, the fine structure of the fluorine atom being also explicitly taken into account. The technique presented is shown to be simple and effective for applications to reactive scattering problems, and the results are competitive with those obtained applying other current methods, especially in the strong triatomic interaction region. © *1998 American Institute of Physics.* [S0021-9606(98)01834-0]

I. INTRODUCTION

In the previous paper, Part I[1] (see also Ref. 2) we have presented a novel treatment to solve the Schrödinger equation in hyperspherical coordinates at fixed values of the hyperradius, which is the reaction coordinate in the time independent hyperspherical approach to chemical reactions. This is a very time consuming step for reactive state-to-state cross-section calculations and the success of the hyperspherical treatment in this field is largely dependent from the solution of the quantization problem on the surface of a multidimensional sphere. The inclusion of excited surfaces is a natural extension of the formalism: the hyperquantization technique allows the easy introduction of the spin-orbit interaction.

We have carried out our calculations on a benchmark system, the reaction F+H₂→HF+H at a total nuclear angular momentum equal to zero. This is the most studied reaction (see Ref. 3 for recent progress) after H+H₂ and is one of the few chemical systems for which exact hyperspherical close coupling convergent calculations of the quantum dynamics have been carried out. All studies have been limited to the dynamics on the ground potential energy surface. The semiempirical T5A surface[4] has been largely used and there are published results obtained with other hyperspherical numerical techniques.[5,6] For purposes of detailed comparisons, the accuracy of the hyperquantization algorithm has been tested on this surface, although some tests on a more recently proposed *ab initio* potential energy surface[7] have also been performed and will be commented on.

The system F+H₂ also offers the opportunity to investigate the role of nonadiabatic electronic transitions in chemical reaction dynamics. The open-shell electronic structure of the fluorine atom leads to multiple electronic states that are asymptotically degenerate in the reactants' valley. Many authors have investigated the nature and the effects of the electronically excited states in this reaction, including decoupling of asymptotic channels,[8] or wave packet propagation,[9] or simplifications such as the restriction to collinear configurations.[10] Lester and Rebentrost[11] developed a complete theory, but for the case of inelastic collisions. Very recently, nonadiabatic reactive cross-section calculations have been carried out for a symmetric system Cl+HCl (Ref. 12) in a spirit similar to ours.

This work reports an account of the performances of the hyperquantization algorithm both in the symmetric and asymmetric hyperspherical coordinate representations. Analytical tools for our technique are generalized vector coupling coefficients (Hahn polynomials) as the discrete analogs of hyperspherical harmonics, and the numerical tool is a Lanczos algorithm to carry out diagonalization of very large and sparse matrices. A large part of the paper will illustrate time and memory requirements as well as the accuracy of the algorithm, providing also a comparison of our results with those obtained by applying other computational methods.[5,6,13] To exhibit the perspectives offered by the technique, we also proceeded to evaluate the modifications of the hyperspherical effective adiabatic potentials because of the introduction of the spin-orbit effect. We have done this by developing a general formalism, extending the reactions to Lester and Rebentrost's treatment, to include the angular momenta relevant to electronic motions, i.e., the total orbital angular momentum and the total spin angular momentum.

The structure of this article is as follows. In Sec. II we describe the electronic characteristics of the reaction and we show how excited potential energy surfaces can be modeled exploiting experimental information obtained in our laboratory from nonreactive scattering between fine structure analyzed F and H₂.[14] The construction of the Hamiltonian matrix is also briefly discussed. In Sec. III we present the results and discuss the accuracy of computed eigenvalues and the efficiency of the hyperquantization algorithm. The conver-

[a]Electronic mail: aquila@hermes.chm.unipg.it

gence rates are explained in light of the topological features of the potential energy surface and the performances obtained for both the symmetric and the asymmetric hyperangular parametrizations are compared. Results are also given for the effect of the inclusion of fine structure. Conclusions follow in Sec. IV. Finally, in the Appendix we report the results of our studies on the currently available Lanczos procedures with reference to their suitability to exploit the specific properties of our algebraic problem and thus to improve upon the performance of the hyperquantization technique. Units in this paper are eV for energies and the Bohr radius a_0 ($=0.529\,177\,06 \times 10^{-10}$ m) for lengths.

II. THE F+H$_2$ SYSTEM

A. Electronic orbital characteristics of the reaction

The principal features of this reaction are well established, because of the large attention received over the years. Although most theoretical efforts have been limited to single surface treatments, there are three doublet potential energy surfaces correlating with reactants and thus relevant also for thermal energy reaction dynamics, namely $1\,^2A'$, $2\,^2A'$ and $^2A''$ in the nomenclature of the symmetry group C_s. For the ground electronic state, $1\,^2A'$, we have employed the T5A surface. Many surfaces for the excited electronic states have been proposed from quantum chemical calculations, and a review is available in the Ref. 9; however, for the long range features of the interaction potentials it is more accurate to make refer to experimentally derived information. Accordingly, we will construct the excited surface using an experimental ''correction'' to the ground one, as has been determined in our research laboratory from scattering measurements of magnetically selected fluorine atoms and hydrogen molecules.[14]

The splitting between the $^2P_{3/2}$ and $^2P_{1/2}$ states of the fluorine atom, due to the spin-orbit effect is equal to 0.0501 eV, which is a very small spacing but crucial for thermal reactivity. The coupling between surfaces induced by both the spin-orbit interaction and the orbital and rotational motions of the nuclei is localized in the entrance channel. This is the region that we will analyze in more detail; in the remainder of the configuration space the excited electronic surfaces are dynamically uncoupled from the ground state. Therefore the explicit consideration of the electronic angular momentum is significant, for this system, only in the asymptotic region of the reactants. In the other regions, such as the product valley and the internal region of strong interaction, the potential decouples the centrifugal and rotational terms from the electronic angular momenta and the reaction proceeds only on the ground surface. We can say that *the potential, in the strong interaction zones, uncouples nuclear and electronic angular momenta.*

On the other hand, in the entrance valley, i.e., in the asymptotic region of the reactants, the hydrogen molecule can be thought as a particle without structure, and the three-body interaction reduces to an effective two-body problem: the potential energy surfaces $1\,^2A'$, $2\,^2A'$ and $^2A''$ reduce to potential curves corresponding to the body-frame components Λ of the orbital electronic angular momentum. Specifi-

cally the ground surface $1\,^2A'$ has a Σ character ($\Lambda=0$) while the excited electronic states $2\,^2A'$ and $^2A''$ both have a Π character ($\Lambda=1$). Since the total orbital electronic angular momentum correlates adiabatically with the orbital momentum of fluorine, the labels Σ and Π hold their validity as long as the atom–diatom separation is large enough that the internuclear axis can be taken as a quantization axis. The Π state acquires an increasingly repulsive character for decreasing hyperradius, so that the surfaces are widely separated in energy.[14] For further developments, it has to be taken into account that both the ground surface and the excited one with $\Lambda=1$ asymptotically correlate with the state ^2P of the fluorine. The degeneracy is removed when the fine structure of the fluorine atom is explicitly considered, and both $1\,^2A'$ and $^2A''$ tend to $^2P_{3/2}$, while $2\,^2A'$ tends to $^2P_{1/2}$.

Let us now illustrate some topological features of the ground potential energy surface ignoring the fine structure of the F atom:[15] the appearance of the ridge [evolution of the minima with respect to Θ (or ϑ) and maxima with respect to Φ (or χ)] delimits the hyperradius values for which it is meaningful to consider channels for reactants and products as separated. For the *ridge* concept, see Refs. 16, 17 and 18. This is an important feature which allows the definition of the region of the configuration space where both the role of excited electronic surface is relevant and the splitting due to the fine structure of the F atom has to be taken into account.

Figure 1 shows the T5A surface at two values of the hyperradius as a function of the angles of the symmetric (Θ,Φ) and asymmetric (χ,ϑ) hyperspherical coordinates, see Ref. 1 for their definition.[1] The topology of the surface varies as ρ changes. At ρ values smaller than $4.5a_0$—which corresponds to the collinear saddle for the reaction—the potential energy surface has the shape of a single bowl. When the value $4.5a_0$ is reached a wall arises to separate the reactants and products valleys, and at larger hyperradius the cuts of the potential exhibit two bidimensional wells separated by a saddle. The ridge line is the evolution along ρ of such a saddle, and divides the two wells corresponding to separated reactants and products. The valley bottom lines are similarly generated as the evolutions of the minima of the potential energy surface as ρ varies. When the hyperradius increases the ridge grows and the minima of the potential are localized in small regions of the interaction space.

The splitting of the potential energy surfaces due to fine structure as a function of the internal coordinates is described introducing experimental information. The symmetric hyperspherical parametrization will be used in the following, although the procedure is general. From scattering experiments carried out in our laboratory,[14] functional forms for the atom–diatom interaction at long range are available. These are given as $V_0(R)$ and $V_2(R)$ as a function of the distance R, the modulus of the Jacobi vector joining the fluorine atom to the center of mass of H$_2$ in the entrance channel. We will not use the experimental $V_0(R)$ explicitly, having been incorporated already in the T5A. The anisotropic component $V_2(R)$ is related to the splitting of the surface into components with Σ and Π character. Explicitly
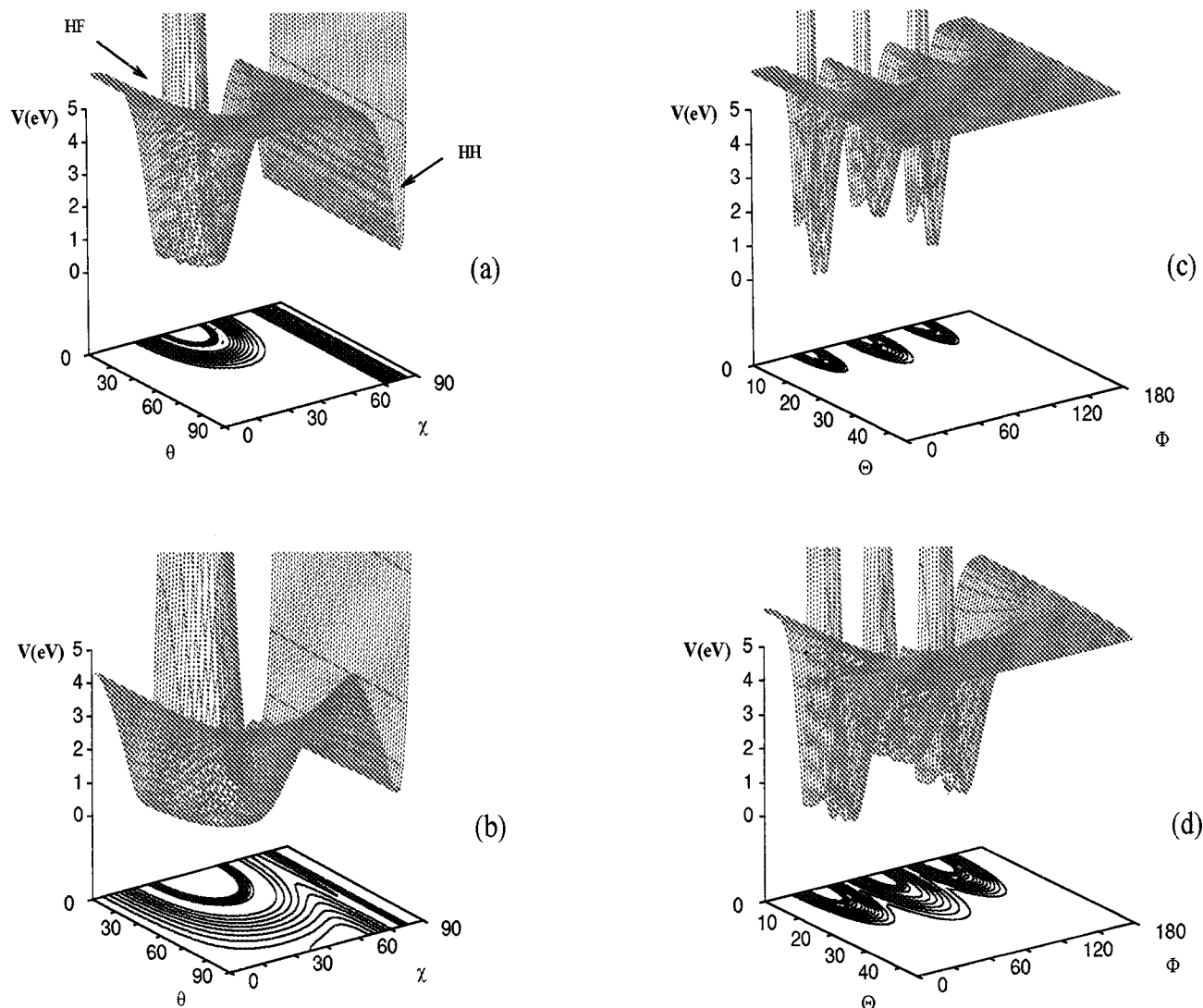
$$V_2(R) = \tfrac{5}{3}[V_\Sigma(R) - V_\Pi(R)]. \tag{1}$$

FIG. 1. Views of the T5A potential energy surface for the reaction F+H$_2$→HF+H. The plots in panels (a) and (b) as a function of the hyperangles ϑ and χ of the asymmetric parametrization referred to the reactants' Jacobi vectors at $\rho=9.0$ and $5.0a_0$, respectively. Panels (c) and (d) are as a function of the hyperangles Θ and Φ of the symmetric parametrization at the same ρ values. For a better perspective we have also plotted the equipotential contour map lines, drawn with a 0.5 eV spacing.

In the entrance channel the H$_2$ molecule acts only as a perturbation on the fluorine atom, and the internuclear distance between hydrogen atoms remains close to the equilibrium value in the molecule, so that we can transform the R dependence of V_2 into a hyperradius dependence. Thus, the excited surface in the entrance channel is given by:

$$V_\Pi(\rho,\Theta,\Phi)=V_\Sigma(\rho,\Theta,\Phi)-\tfrac{3}{5}V_2(\rho), \qquad (2)$$

where V_Σ is the ground state potential energy surface—the T5A in most of our computations. This treatment has to be applied only in the reactants' channel: for decreasing hyperradius, the Π surface increases so much in energy that it becomes decoupled from the ground state. Because of the local representation of the potential matrix in the hyperquantization algorithm, this decoupling can be very easily effected in our formalism (see below). Note that in terms of the internal angles of the symmetric hyperangular parametrization, the $\Sigma-\Pi$ separation here is properly considered independent of Θ (being only due to the internal structure of the

fluorine atom), while it depends on Φ, which is the angle which spans the range among the reaction channels. For simplicity, the dependence on Φ will therefore be modeled below as a step function. Similarly, a switch-off of the spin-orbit coupling will ensure its neglect in the exit channel. Any other choice for the angular dependence would not complicate the numerical implementation, but the simple ones chosen here are sufficient to guarantee inclusion of all the reliable information presently available, as well as of all features relevant for the dynamics.

B. The Hamiltonian matrix structure and the spin-orbit effect

The hyperquantization technique allows us to easily extend the theory and formalism in order to include the spin-orbit interaction, which provides the coupling between the potential energy surfaces. Results of quantum scattering calculations in the multisurfaces case will be shown in Sec.

III C. The following formulation can be considered a generalization of that presented in Ref. 1 for the single surface case, and reduces back to it if one includes only one electronic state. In the following, we will analyze equations written in terms of the variables of the symmetric hyperangular parametrization.

In the collision between an open-shell atom with a diatomic molecule, the true physical invariant of the system is the vectorial sum of angular momenta related to both electronic and nuclear motions, as well as spin. So nuclear and electronic contributions to the total angular momentum are not separately conserved. This is an implicit approximation in the single-surface treatment of the scattering: the Born–Oppenheimer model separates nuclear and electronic dynamics, and the relative angular momenta are considered separately conserved. The allowed values of the total (nuclear plus electronic) angular momentum are half-integer because of the doublet character of the surfaces (the total spin S is 1/2) and the lowest allowed value is thus 1/2.

In Ref. 1 we have shown that the orthogonal transformations on the eigenvectors performed in the application of the hyperquantization algorithm drastically change the structure of the matrices. In the multisurfaces extension, application of the transformations involves only the nuclear part of the basis functions and the presence of two electronic states causes only the appearance of the corresponding blocks and the relevant coupling matrix elements. The previous treatment of the single surface case, limited in Sec. III of Ref. 1 to zero total angular momentum, is here extended and illustrated for direct comparison only for zero value of the projection of the total *nuclear* angular momentum on the principal maximum inertia axis.

The presence of the excited electronic state and of the spin-orbit term on the total Hamiltonian of the system modifies the structure of the quantization problem at fixed ρ as follows:

$$\sum_{\Lambda'\tau'\nu'} [K_{\Lambda'\tau\nu\tau'\nu'\Lambda'}\delta_{\tau\tau'}\delta_{\tau\tau'\pm1} + V_{\Lambda'}(\rho,4\Theta_{\tau'},2\Phi_{\nu'})\delta_{\tau\tau'}\delta_{\nu\nu'}$$

$$+ V^{so}_{\Lambda\Lambda'}(\rho,4\Theta_{\tau'},2\Phi_{\nu'})\delta_{\tau\tau'}\delta_{\nu\nu'}]t_{i\Lambda'\tau'\nu'}(\rho)$$

$$= \varepsilon_i(\rho)t_{i\Lambda\tau\nu}(\rho). \tag{3}$$

Apart from the spin-orbit term $V^{so}_{\Lambda\Lambda'}$, there is an absolute analogy with the previously treated single surface case, see Eq. (54) in Ref. 1, the difference being the appearance of the Λ and Λ' labels for the ground and excited electronic states, corresponding in the two surface case to Σ and Π, respectively. The eigenvalues ε_i asymptotically correlate in the entrance channel with the rotovibrational energy levels of the H_2 molecule in the ground electronic states, and the fluorine atom is either in the $^2P_{3/2}$ or in the $^2P_{1/2}$ state. The Hamiltonian matrix is schematically composed of four blocks, the spin-orbit couplings appearing in the two identical off-diagonal blocks. All the information for the motion of the three-atom system in the ground and excited potential energy surfaces is separately contained in the two blocks along the main diagonal: the kinetic energy matrix has a block-tridiagonal structure and the potential energy matrix is diag-

onal, its elements being the values of the ground or excited potential surfaces at the grid points. The construction of each of these matrices follows the procedure outlined in Ref. 1. Recall that the elements of kinetic energy matrix depend on ρ simply as $1/\rho^2$ and therefore it is not necessary to calculate them again when the same grid is used at different values of the hyperradius. The high symmetry and sparseness make practically negligible the time which the code takes to construct the Hamiltonian matrix, time requirements being essentially determined by the computation of the values of the potential energy surfaces at the grid points.

The spin-orbit coupling matrix $V^{so}_{\Lambda\Lambda}$, arises because of the spin-orbit interaction, which operates only when the fluorine atom can be thought as a separate species, and therefore its role has to be limited to the reactant's channel. As before for the $\Sigma - \Pi$ splitting, we consider the spin-orbit interaction independent of the angle Θ, which is the collective coordinate corresponding to the triatomic bending motion in the normal mode picture. This mode is not effective in the reactants' channel where the H_2 molecule is effectively a single particle. The couplings due to the spin-orbit interaction are different from zero only for those values of the hyperradius and of the kinematic rotation angle Φ corresponding to the reactants' channel. This variable plays a decisive role in order to define the progress of the reaction; as is evident from panels (c) and (d) of Fig. 1, it scans progressively the different rearrangement channels. The dependence on the internal coordinates of the $V^{so}_{\Lambda'\Lambda}$ term is therefore factorized as follows:

$$V^{so}_{\Lambda'\Lambda}(\rho,\Theta,\Phi) \sim V^{so}_{\Lambda'\Lambda}(\rho)H(\Phi), \tag{4}$$

where $V^{so}_{\Lambda'\Lambda}(\rho)$ are given in Hund's case (c)[19] (see also Ref. 9)

$$V^{so}_{\Sigma\Sigma}(\rho)=0 \quad V^{so}_{\Sigma\Pi}(\rho)=-\frac{\sqrt{2}}{3}\,\delta,$$

$$V^{so}_{\Pi\Sigma}(\rho)=-\frac{\sqrt{2}}{3}\,\delta \quad V^{so}_{\Pi\Pi}(\rho)=\frac{1}{3}\,\delta, \tag{5}$$

where δ is the fluorine atom spin-orbit splitting. The dependence on Φ is described by a Heaviside's stepwise function

$$H(\Phi)=\begin{cases} 1, & \text{for } \Phi_{ridge}\leqslant\Phi\leqslant\pi/2 \\ 0, & \text{for } 0\leqslant\Phi<\Phi_{ridge} \end{cases}, \tag{6}$$

where Φ_{ridge} indicates the particular value of the kinematic angle Φ corresponding to the ridge line, which marks the separation between the valleys of reactants and products.

As for the dependence of the coupling terms on ρ, being the spin-orbit interaction a property of the fluorine atom, it is expected to switch off when the atom loses its chemical identity for small hyperradius values. The disappearance of the ridge, which occurs at $\rho\sim4.35a_0$, marks a critical value for the hyperradius, because the distinction between separated channels for reactants and products of the reaction disappears for smaller ρ. However, there the $V_\Sigma-V_\Pi$ separation is so large that the spin-orbit coupling becomes negligible and in our formulation it is switched off automatically.

Since the spin-orbit matrix is formally identical to a potential energy matrix, all the nonzero elements are placed along the diagonals of each Λ block and assume the values corresponding to the grid points labeled by τ and ν. When, as assumed here for simplicity, the terms are constant as a function of Θ, all blocks are equal with respect to the τ index and show the simple dependence on Φ previously examined. Each τ block has nonzero elements only in correspondence to specified ν indices, which thus localize the Φ values in the range included between the ridge and the extreme of the allowed angular domain.

In general, consideration of the spin-orbit interaction as effective in all configurations space, and explicit information of its dependence, formally involves only a proper filling up of the diagonals of the τ blocks, with no change in the matrix structure. Obviously, such a detailed knowledge of the complete spatial dependence of the $V^{so}_{\Lambda'\Lambda}(\rho,\Theta,\Phi)$ terms is not currently experimentally available, and moreover sufficiently accurate relativistic quantum chemical calculations are out of reach at the present time. Nevertheless, this formulation can be immediately implemented to cope with progress in this direction.

C. The computation of generalized vector coupling (Hahn) coefficients

As emphasized in Ref. 1, the hyperquantization technique is based on the use of the discrete analogs of hyperspherical harmonics. These are products of polynomials of a discrete variable orthogonal on a set of grid points, Hahn coefficients. Such polynomials[20] can be identified with $3j$ (and generalized $3j$) symbols where the number of grid points, I and N, appear as artificial angular momenta and the discrete variables τ and ν are their projections. The Hahn coefficients enter into the expressions of both the kinetic energy matrix elements and the overlaps between eigenvectors of adjacent sectors when the dimension of the grid is changed, see Eqs. (42), (57) and (73) in Ref. 1. However their explicit calculation is required only for the overlap matrices in the propagation step, since in the construction of the kinetic energy matrix the problem is solved analytically. We have found it important, especially envisioning the extension of the hyperquantization methodology to chemical systems with more than three atoms, to implement a routine capable of evaluating accurately all Hahn polynomials, i.e., both the $3j$ and generalized $3j$ symbols.

From a study of the numerical stability of the most frequently used algorithms for $3j$ symbols, it appears that the computational techniques based on the exact solution of a recurrence equation are the most efficient and accurate. The routines that exploit conventional close formulas[21] fail for large j. None of the six explicit expressions known for the vector coupling coefficients in the form of algebraic sums,[22] as well as their manipulations such as a recent one,[23] is stable when large quantum numbers ($\gtrsim 10^2\hbar$) are used: there is a loss of precision due to the alternating signs in the sums which limits their range of applicability. The improvements suggested in Ref. 24 as well as the nested forms used in Ref. 25 do not solve the problem fully. Some little improvements

have also been obtained in our group through an algebraic manipulation of these sums; however the loss of significant figures can be attenuated but not eliminated. Also the routines based on the semiclassical formulation of Schulten and Gordon[26] are not competitive with the recurrence ones, developed and exploited by the same authors,[27,28] particularly when a complete set of $3j$ coefficients is needed, as in our applications.

The $3j$ coefficients of very high ($\gtrsim 10^3\hbar$) angular momenta can span many orders of magnitude. In order to ensure numerical stability the choice of the point where forward and backward recursions are matched is crucial, and it is very important to start the recurrence from a small value of the entry and to end up in a large one. To gain stability in the calculations, we have extended to generalized $3j$ symbols the original routine of Schulten and Gordon,[27,28] but before starting the recursion we implement the determination of the classical regions for the $3j$ coefficients. The classical regions as defined in Refs. 26 and 27 are the sets of j values for which there exists a classical angular momentum vector diagram corresponding to the $3j$ coefficient. The matching point of the forward and backward recursion is chosen at the boundary of the classical and the quantum regions, where the string of the $3j$ coefficients always has a large maximum. With this choice and with the numerical strategy of Ref. 28 to prevent underflow and overflow problems, we can perform calculations for arbitrary large quantum numbers (we have performed tests for angular momenta as large as $10^4\hbar$ and checked them by monitoring the orthogonality of the coefficients obtained). A similar approach has been used to build a routine that exploits an analogous three term recurrence equation, extended to allow the calculation of generalized[20] $3j$ symbols. This routine evaluates explicitly the Hahn coefficients used in the hyperquantization algorithm.

III. RESULTS AND DISCUSSIONS

A. Convergence

In the following we investigate the convergence of fixed ρ eigenvalues for the $F+H_2$ reaction in both the *symmetric* and *asymmetric* hyperspherical coordinate representations, corresponding to the couples of angles Θ,Φ and χ,ϑ, respectively. Numerical techniques are discussed in the Appendix. Electronic orbital and spin-orbit effects will be neglected until Sec. III C.

The study of the convergence of eigenvalues as a function of several parameters is a complex work. As stressed in Ref. 1, in the hyperquantization algorithm there are four parameters to be specified: the number, I, of grid points for χ or Θ which gives the number of blocks of the Hamiltonian matrix; the number, N, of grid points of ϑ or Φ which defines the dimension of a single block; the cut-off parameter for the potential, V_{max}, which controls the dimension of the matrix by establishing an upper limit for the energy range; the D_{corner} parameter which fixes the number of diagonals whose elements are to be kept different from zero in each block. It is important that the convergence as a function of each parameter be as uncoupled much as possible from the convergence of the others. The rate of convergence depends

TABLE I. Parameters for the convergence of ''production runs'' as a function of ρ.[a]

ρ (a_0)	I	N	V_{max} (eV)	D_{corner}
9.00	5000	200	4.6	20
7.00	3000	160	4.6	20
5.00	1600	120	4.6	20
4.00	600	80	4.1	25
3.50	300	90	5.2	25
3.00	1000	100	8.0	40
2.20	1500	100	20.0	50

[a]The data are referred to the calculations in symmetric hyperspherical coordinates.

TABLE II. Features of Hamiltonian matrix as a function of ρ.

ρ (a_0)	Final dimension[a]	Nonzero elements[b]	% sparseness
	Ground electronic state (Σ)		
9.00	100341 (80)	3 989 787 (42)	0.040
7.00	99703 (59)	4 526 726 (40)	0.045
5.00	86085 (12)	4 154 909 (42)	0.056
4.00	21243 (14)	613 847 (41)	0.136
3.50	11696 (14)	507 847 (24)	0.371
3.00	42247 (18)	2 718 823 (5)	0.152
2.20	60041 (22)	3 938 417 (0)	0.109
	Excited electronic state (Π)		
9.00	13177 (97)	251 862 (0)	0.145
7.00	14665 (94)	339 635 (0)	0.158
5.00	13130 (88)	252 488 (0)	0.146

[a]After reduction by the V_{max} parameter, to be compared with $(I+1)(N/2+1)$ with N and I as in Table I; in parenthesis, percent reduction.
[b]After reduction by the D_{corner} parameter; in parenthesis, percent reduction.

on the particular eigenstate[13] and one is easily mislead if only some eigenvalues are watched to find the optimal parameters. As shown in Fig. 1, the topology of the potential energy surface varies significantly as ρ increases and in order to determine the optimal parameters used in ''production runs'' the convergence has been tested at several representative values of ρ. The results proved that the hyperquantization technique is more efficient and accurate when the hyperspherical symmetric angular coordinates are used, so in the following we first discuss this parametrization. This superiority of the symmetric representation is probably true in most cases and for most numerical techniques, but this appears to be the first systematic investigation.[29]

1. Symmetric hyperangular parametrization

In *symmetric hyperspherical coordinates*, at all ρ values the convergence of all eigenvalues is from above with respect to I while with respect to N the correct values are reached from below. No reason can be given for this variational-like versus nonvariational-like behavior. In general, we observe that the convergence is slow as I increases, especially at large ρ, and very sharp as N varies; with respect to the latter parameter, 4–5 significant figures are obtained very easily. The convergence with respect to V_{max} is variational and fast, and obviously the highest eigenvalues are more affected from this parameter. The convergence with respect to D_{corner} is random, the eigenvalues converging both from above as well as from below. The convergence rate results are uncoupled if reasonable values are chosen for the other parameters and it varies smoothly in the whole range of ρ.

In Table I we give the actual parameters used in the ''production runs'' at some selected ρ values and in Table II we list the dimension of Hamiltonian matrix, the number of elements different from zero and the efficiency of the reduction on these quantities produced by V_{max} and D_{corner}, and the global sparseness of the Hamiltonian matrix, defined as the number of nonzero elements divided by the total. The data refer to the calculation of the first 150 eigenvalues which in a benchmark calculation[13] are considered necessary to obtain converged reaction probabilities at thermal energy.

The required parameters I and N attain their smallest values at ρ around $3.5a_0$, (see Table I) and there the Hamiltonian matrix to be diagonalized has the smallest dimension. However, there the extent of the reductions in number of

zero terms due to V_{max} and D_{corner} is less efficient than at higher ρ values (see columns 2 and 3 in Table II), being the potential energy surface is delocalized in a large area of the interaction region.

As ρ approaches the asymptotic limit, the portion of the potential energy surface relevant to the reaction is confined in the rearrangement channels of reactants and products, where eigenvectors have a substantial amplitude, and our algorithm requires larger values of N and I to achieve convergence; nevertheless, the effective dimension of the Hamiltonian matrix, i.e., after the V_{max} and of D_{corner} reductions, doesn't vary much. In fact, at large hyperradius the cost of the increased values of I and N is balanced by the benefit of the higher efficiency of both the potential cut-off V_{max} and the D_{corner} parameter; regarding the latter, 20 subdiagonals for each block suffice to ensure the convergence of eigenvalues.

At the smallest ρ values the cut-off for the potential is less efficient and reduces slightly the dimension of the matrix; the reduction of the nonzero elements due to D_{corner} is also modest: the surface of the hypersphere is smaller, the discrete variable ν labels points spatially very close and the motion of the system is highly coupled in the ν quantum number. From the last column of Table II we can see that, despite the large matrix dimension, only less than one in 10^3 of the elements are different from zero and this number varies only slightly as the hyperradius increases. This high sparseness is crucial both for the time and memory requirements of the whole calculation.

The observed fast convergence of the eigenvalues with respect to the grid for the Φ variable leads to relatively small values of N, and correspondingly to small dimensions for the blocks of the kinetic energy matrix. The number of nonzero elements grows as the square of N and therefore a reduction of the N value leads to a substantial increase in the sparseness of the matrix, increasing the efficiency of the hyperquantization algorithm.

The data in Table II refer to the Hamiltonian matrix for the ground and excited electronic states. Two independent calculations on the two surfaces are carried out ''adiabati-

cally,'' i.e., separately; the couplings due to the spin-orbit interaction are later included and the complete Hamiltonian matrix is diagonalized. This is done only for hyperradius values larger than $5a_0$, because below this value the spin-orbit interaction is substantially quenched. For the excited surface, convergence on grid points is observed to follow the same pattern as for the ground surface. However, the potential cut-off $V_{\max}$ for the excited surface now has a greater effect and the corresponding electronic block is drastically reduced. This reduction is decisive to permit the inclusion of the excited surface in the calculations. At small hyperradius, and in general outside of the entrance channel, the upper electronic state grows rapidly in energy, so that the corresponding surface does not contribute to the description of the chemical reaction. This behavior enables us to localize the electronically nonadiabatic effects (such as the spin-orbit treated here) in the region where the excited surface is modeled as outlined in Sec. II A. All the other regions of the hypersphere are eliminated by the potential cut-off procedure. So, the dimensions of the electronic blocks of the Hamiltonian matrix differ, the one corresponding to the electronic excited state being much smaller, and conserving only the values of grid points labeled by ν and τ which localize the reactants' channel on the hypersphere, other pairs ν,τ having been eliminated.

2. Asymmetric hyperangular parametrization

The situation is quite different in the *asymmetric representation* (here we refer to a hyperspherical coordinate parametrization of Jacobi vectors for the reactants channel, in order to exploit the exchange symmetry of the H_2 molecule. For other choices, see Ref. 30). Figure 2 illustrates the convergence of several representative ground surface eigenvalues as a function of the number of grid points for the hyperangle χ at $\rho = 9.0a_0$ and $N = 200$. At this ρ the reactant and product valleys are well separated: the eigenvalues are close in energy to rotovibrational spectra of H_2 and HF and the corresponding eigenfunctions give a unity overlap with diatomic rotovibrational wave functions to the fourth decimal place. For most eigenvalues the convergence is from above with respect to I but from below as the N parameter increases. Figure 2 illustrates patterns which are manifest in the whole range of ρ and make convergence slow. The figure shows that the third significant figure is reached quickly, but a large effort is required for the fourth digit which ensures the correct sequence of the eigenstates.

We attribute such a slow convergence rate to specific features of the potential energy surface in the asymmetric hyperangular parametrization, see panels (a) and (b) in Fig. 1. In our technique, the interaction region is represented by a grid of equally spaced points in both $\cos 2\chi$ and to $\cos \vartheta$ [see Eqs. (66) and (67) in Ref. 1]. So, when hyperspherical asymmetric coordinates are employed, the reactants and product channels are confined in small areas of the shape space where the set of grid points has the largest spacing with respect to the the angles χ and ϑ. Consequently, in order to obtain convergent eigenvalues correlating with the H_2 rotovibrational spectrum we need a very large value of I, while to obtain the eigenvalues correlating with the HF ro-
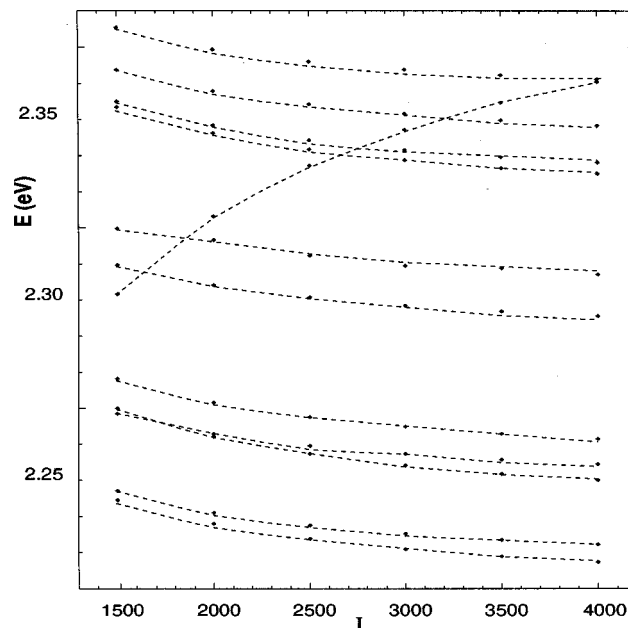

FIG. 2. Convergence rate of eigenvalues as a function of the I parameter (grid points for θ) for the asymmetric parametrization of the reactants' Jacobi vectors at a fixed value of χ grid points ($N = 200$) and $\rho = 9.0a_0$. A set of eigenvalues which converges to three figures is placed on top of a set of not converged eigenvalues: the first set has a variational convergence with the eigenvalues approaching their stable value from above while the other set shows a nonvariational convergence. These patterns appear starting from about 2 eV when the H_2 channel is opened and arise more frequently when the energy increases. If I is not large enough the correct sequence of eigenvalues and their adiabatic correlation with the rotovibrational molecular levels are missed. At larger energies with respect to the ones shown, the situation is worse and it is very difficult to draw conclusions because too many crossings appear.

tovibrational spectrum a large value for N is necessary. These observations show the limitations due to the use of the asymmetric parametrization, even if one tries to exploit the freedom of choice for the kinematic rotation. Panels (c) and (d) in Fig. 1 show pictorially the advantages of the symmetric hyperangular parametrization.

Although minor accuracy is in general achieved for the asymmetric hyperangular parametrization, we remark that in this study only the hyperspherical harmonics relative to one set of Jacobi coordinates is included in the expansion of the wave function to describe the whole reaction. The performance of the asymmetric representation can be improved by using as an *overcomplete basis* the discrete harmonics relative to the Jacobi coordinates of both reactants and products channels. A computation of the eigenvalues correlating with the H_2 rotovibrational states has shown that an order of magnitude in the CPU time is gained with respect to the calculation in symmetric hyperspherical coordinates, the identification of the molecular states being made through the overlaps of the corresponding eigenvectors with the asymptotic channel functions, as described in Ref. 31. At $\rho = 9a_0$ the overlaps are within a few units in 10^3 and the interaction of the F atom with the H_2 molecule is nearly independent from ϑ; correspondingly with respect to this variable a small set of grid points ($N = 20$) is required to ensure very high convergence for the perturbed H_2 states.

TABLE III. Comparison of CPU times between the hyperquantization algorithm (t_{HA}) and the discrete variable representation (t_{DVR})[a] at four ρ values.[b] The ordering number i for the eigenvalues, the corresponding energies ε_i in eV and their percent accuracy with respect to the DVR energies are presented in columns 4, 5 and 6, respectively.

ρ (a_0)	t_{HA}(min)	t_{DVR}(min)	i[c]	ε_i(eV)[d]	% accuracy[e]
2.200	10.7	10.4	1	6.9173	−0.006
			5	7.4935	+0.01
			10	8.2472	−0.03
			$\bar{\varepsilon}(10)$	7.5977	+0.004
3.038	7.5	12.3	11	1.9845	0.000
			15	2.1273	−0.009
			20	2.3201	+0.02
			$\bar{\varepsilon}(20)$	1.8551	0.000
4.975	15.3	16.6	91	2.0724	+0.1
			95	2.1109	+0.08
			100	2.1909	+0.07
			$\bar{\varepsilon}(100)$	1.3985	+0.06
7.299	16.8	13.7	91	2.0587	+0.09
			95	2.1115	+0.08
			100	2.1623	+0.07
			$\bar{\varepsilon}(100)$	1.3800	+0.07
9.000	17.2	8.7	91	2.0764	+0.08
			95	2.1175	+0.1
			100	2.1563	+0.01
			$\bar{\varepsilon}(100)$	1.3801	+0.07

[a]See Ref. 13.
[b]Times have been carried out in symmetric hyperspherical coordinates. t_{HA} are present results taken on a RISC 5000 3AT and t_{DVR} are from Ref. 13 and were taken on a SUN Sparc 2.
[c]Ordering number of eigenvalues.
[d]Calculated energies in eV.
[e]With respect to corresponding DVR results.

Because of the high localization of the wells at $\chi=0$ and $\chi=\pi/2$ [see panel (b) in Fig. 1] many points in the χ angle ($I\sim30\,000$) are required, nevertheless the sparseness of the matrix increases considerably and the calculation time requirements shrink. The CPU time is only 1.5 min, to be compared with 17.2 min which is the time in the symmetric case, see Table III. Obviously, together with accurate H_2 eigenvalues we obtain very poorly convergent eigenvalues for the HF molecule. In order to have a quantitative accuracy also for HF eigenstates another diagonalization has to be made: it is also convenient to use a set of grid points referred to as the Radau vectors,[30] which treat symmetrically the two H atoms, because in these coordinates the potential energy surface is symmetric with respect to $\chi=\pi/4$. The calculation in the asymmetric representation can be made very fast and accurate in the asymptotic region if the discrete harmonics relative to the two different sets of Jacobi coordinates are used to obtain eigenstates correlating with reactants and products channels, respectively.

The main difficulty in the use of an overcomplete discrete basis is the calculation of the overlap matrix between different asymmetric coordinates. The hyperquantization technique allows us to make this projection.[1] We conclude that in the whole range of the hyperradius the symmetric hyperangular parametrization is more appropriate to carry
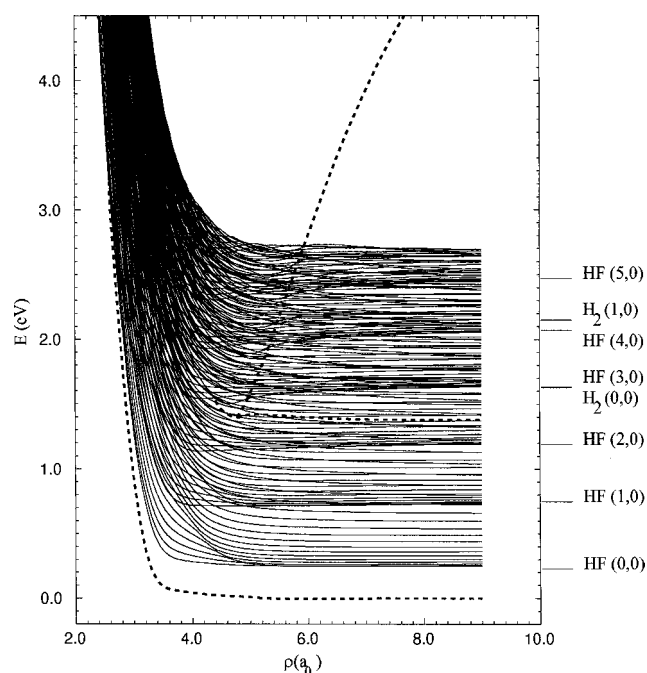

FIG. 3. Fixed ρ eigenvalues for the ground potential energy surface of the reaction $F+H_2\rightarrow HF+H$, $J=0$, as computed for a grid of 136 values of ρ spaced by $0.05a_0$. The calculation has been made in symmetric hyperangular coordinates in the whole range of ρ. The valley bottom curves which support the entrance and exit channel and the ridge curve which marks their separation are also drawn (dashed lines). The lowest rotational states of the rotovibrational spectra of H_2 and HF are indicated.

out numerical calculations of eigenstates than the asymmetric one which parametrizes only one set of Jacobi vectors. An interesting perspective is to use the symmetric coordinates and the corresponding discrete harmonics in the strong interaction region and when the ridge of the potential is high enough to apply separately the hyperquantization technique in asymmetric coordinates for each reaction channel.

B. Comparison with other algorithms

The calculated 150 energy levels for the ground state as a function of the hyperradius for zero total nuclear angular momentum are shown in Fig. 3. At all the 136 values of ρ, the eigenvalues are fully convergent to ±0.001 eV which is a typical accuracy required for scattering calculations. In this subsection we compare our computed energies and CPU time with numerical results obtained with other existing methods for which published eigenvalues[13] exist. In order to cover the whole domain of the hyperradius a comparison has been made at five different values of ρ: two of the chosen values are in the strong interaction region, where the modes of the three atoms resemble those of a triatomic floppy molecule, and the other three are in the long range region, where the system separates asymptotically in the reactant and product valleys. The particular eigenvalues chosen are the central and the two extreme values of the energy intervals given in Ref. 6. They are considered to be most relevant for the reactivity. The average of the first i eigenvalues, $\bar{\varepsilon}(i)$, is also shown as a convenient measure of the overall comparison of the methods. The results of the comparison are shown in

Table III. As reference energies and CPU time we take the values obtained using the discrete variable representation (DVR),[13] since the hyperquantization algorithm has some common features with this method and so it is the most natural one to compare with. However, the comparison with analytic basis method (ABM) and finite elements method (FEM) is straightforward having these techniques already been compared with DVR, see Ref. 6.

At the shortest considered hyperradial distance ($\rho = 2.2a_0$), setting the ''production run'' parameters at the values reported in Table I, we obtained eigenvalues convergent to 4–5 figures. The comparison of the first ten eigenvalues with the published results[6] shows that most energy levels coincide with the fourth digit, even though exceptions occur: some of them coincide with all figures and some others only to three figures. The highest deviation (0.01%) is observed for the tenth state. The motivation of this difference is unknown to us but we claim four convergent figures for this eigenvalue. Our computed eigenstates and also the mean energy are always within the DVR and ABM energies, the latter method being a variational one. The agreement obtained is accurate enough for meaningful comparisons of scattering calculations.

At $\rho \approx 3a_0$ the agreement is excellent, for all the ten eigenvalues of Ref. 6 being within a few tenths of a meV. The mean energy and a large number of eigenvalues coincide with all five digits. In this region of strong triatomic interaction, where reactive channels begin to open within a small ρ range, many avoided crossings occur and the ''adiabatic'' curves are strongly coupled. As stressed in Sec. II A, here the dynamics of the system are still fully triatomic in nature: the ridge line has not appeared yet and the potential energy surface looks like a bowl.

When the hyperradius increases the situation changes. At $\rho \approx 7.3a_0$ the system approaches the asymptotic configurations and the reactant and product valleys are separated. Eigenvalues convergent to five figures are obtained very sharply for all the ''production run'' parameters except for the number of grid points in the Θ angle. As shown in panel (d) of Fig. 1, at large ρ the perturbed diatomic wells are localized around $\Theta \approx 0$ where, being the grid is equally spaced in $\cos 4\Theta$, our algorithm requires a large effort. The convergence with respect to I is very slow and in order to get eigenvalues with an accuracy on the order shown in Table III we have to increase greatly such a parameter. In Table III, the latter ρ value is presented for completeness being the results are similar to those obtained at the previous hyperradius. In the asymptotic region, our eigenvalues are higher in energy than the ABM values and therefore they are less accurate even though this accuracy appears to be sufficient to perform converged scattering calculations.

Timing the comparison of different methods taken on different machines is always very delicate. The comparison is only qualitative and obviously depends on the level of optimization of the numerical codes. Our codes are probably less optimized than those of more consolidated programs and this fact can change the timing by a significant factor. In our algorithm the CPU time is practically governed by the diagonalization time, which is strongly dependent on the particular

Lanczos method used. As illustrated in the Appendix, when a spectral transformation is employed the time and the memory are strictly dependent on the algorithm used to solve the set of linear equations, even though the Lanczos method is the same. Also the way in which the data are stored is very important to determine the Lanczos performance. In our code these steps are not optimized (see Appendix). With the STLM package used in our extensive calculations large temporary direct access files are written and read continuously from the code. Most of the CPU time is spent performing this operation, which is largely dependent on the full architecture of the machine, thus making an absolute comparison of the speed processor of limited significance.

Even though an absolute comparison of the efficiency of different methods is not possible, some qualitative features can be compared. The CPU time required for the diagonalization is linearly proportional to the dimension of the matrix and as a function of ρ shows a pronounced minimum around $3.5a_0$. In the interval $3.0a_0 \lesssim \rho \lesssim 4.5a_0$ the motion of the particles is effectively triatomic in nature and our algorithm results are very efficient: convergence is fast and the accuracy of the eigenvalues is even better than that listed in Table III for the two smallest ρ values. At these values of ρ, there are no published results for comparison, but from the CPU times reported in Refs. 6 and 13 we see that they do not show any significant change until the value $\sim 5a_0$ is reached. Below $3.0a_0$ the CPU required increases rapidly. From a numerical point of view this difficulty is not too serious, because in this region the eigenvalues are very high in energy and a lower level of accuracy is necessary to have converged reactive probabilities. We conclude that for values of $\rho < 4.5a_0$ our algorithm can be competitive with the other ones.

At hyperradius values larger than $4.5a_0$ the CPU time is roughly constant. As stated in the previous subsection, at large ρ the minima of the potential energy surface are very localized on the hypersphere and more points of the angular variables are necessary to describe the eigenfunctions causing an increase in the dimension of the matrix. For the same reason there is a proportional increase in the reduction efficiency of the V_{max} parameter and this yields a compensation between the two effects. Typically, the dimension of the matrix is such ($\approx 10^5$) that about 17 min of CPU are necessary for the diagonalization. As will be shown elsewhere, the introduction of a suitable basis contraction scheme of the diagonalization-truncation type, reduces these times by an order of magnitude. A comparison with our method should be done with the asymmetric hyperspherical coordinates using an overcomplete basis as well. The hyperquantization technique allows this extension, but this methodology has not been fully implemented yet and we delay this comparison to a future work.

Figure 3 shows the 150 single surface eigenvalues as a function of ρ obtained at $J=0$ for this reaction considered on the ρ range necessary to obtain converged reaction probabilities. For the computation of these curves and the corresponding matrices of eigenvectors we have used a constant ρ grid of 136 points giving sectors $0.05a_0$ wide. This hyperradius grid includes more points than that used in typical calcula-

tions on the same potential energy surface. As a function of the hyperradius, I and N have been varied, but the same grid has been kept for several sectors. Practically, we found it appropriate to change the grid when ρ increases $1a_0$ in the interval $5.0–9.0a_0$. In the range $2.2–5a_0$, I and N had to be changed more rapidly as ρ varies and we found it necessary to change the grid when ρ varies by $0.5a_0$.

On the same plot the rotational ground states of the rotovibrational spectra of H_2 and HF are indicated to show the relevant energetics of the various channels for the reaction. We have also drawn the ridge and valley bottom curves of the T5A surface. At ρ around $6.0a_0$ the ridge is higher than the 150th eigenvalue; beyond this point the reactivity is very small and the eigenvalues are close to the reactant and product rotovibrational spectra.

C. Fine structure effects

In this section we present the results obtained including the upper surface and the spin-orbit coupling, i.e., solving the fixed hyperradius problem of Eq. (3). We use the symmetric hyperangular parametrization. These calculations provide the eigenvalues ε_i correlating at large ρ with the entrance channels with the fine structure, i.e., to a specific rotovibrational state of the H_2 molecule and the F atom in the states $^2P_{1/2}$ and $^2P_{3/2}$. Here our aim is to study the computational aspects involved in this extension, which yield essentially the modification of the effective potentials shown in Fig. 3, because of the introduction of the upper surface and of the spin-orbit interaction. This determination of the modified potentials $\varepsilon_i(\rho)$ is a first step towards the evaluation of the role of electronic orbital and fine structure effects.

The present test calculations were performed at a total angular momentum value 1/2, for the projection of the nuclear angular momentum equal to zero. This allows a direct comparison with the results of the previous section, obtained for the single surface case. Separate calculations for the two surfaces at the asymptotic value $\rho = 9a_0$ allow us to obtain, in addition to the 150 eigenvalues supported by the Σ potential energy surface, 13 additional curves on the Π surface, higher states not being accessible at thermal energy. In the hyperspherical description of quantum collisions, these states contain all the information on the role of the excited surface on dynamics.

At the largest value studied of the hyperradius $\rho = 9a_0$, the energetic gap between electronic states, both correlating asymptotically to the same state ^2P of fluorine atom, is smaller than the fine structure splitting. In internal regions (smaller ρ), the excited surface rises in energy, and correspondingly the eigenvalues exit from the energetic range relevant for thermal reactivity.

In Fig. 4 curves obtained from diagonalization of the complete matrix (including spin-orbit) are shown, for the $5–9a_0$ hyperradius range. For smaller ρ values, all the eigenvalues on the upper surface exit out of the interesting spectral range, and results become the same as in the single surface case. This is a manifestation of the quenching of the spin-orbit effect in the strong interaction region, where the fluorine atom electronic structure is lost.
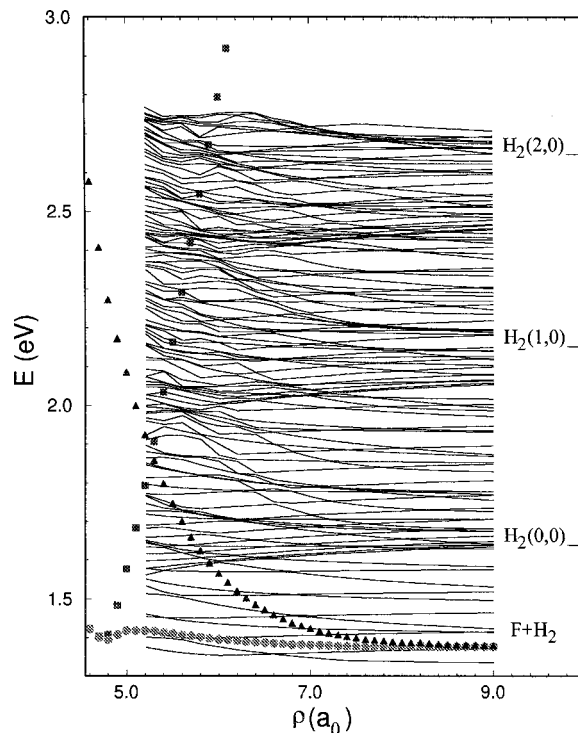

FIG. 4. Adiabatic eigenvalues obtained from the diagonalization of the complete Hamiltonian matrix: only the hyperradius range $5–9a_0$ significant to illustrate the open-shell and the spin-orbit effects is shown. Squares define the ridge line, circles and triangles the valley bottom of the T5A and excited surface, respectively. The vibrational ground and two excited states of the H_2 molecule are indicated.

Since the reactivity is over beyond $\rho > 6a_0$, the eigenvalues there tend to their asymptotic values, the rovibronic states of reactants and products, and to the fine structure levels of fluorine. The results show, as expected, no change in the eigenvalues correlating with the product HF. The effects of the atomic open-shell and of the spin-orbit coupling manifest in the entrance valley, and the asymptotic correlation between calculated eigenvalues and the molecular states of H_2 are shown in Table IV, where data refer to the largest investigated ρ value, $9a_0$.

TABLE IV. Eigenvalues (eV) at $\rho = 9.0a_0$ correlating with specific H_2 rotovibrational levels (v,j), calculated on surfaces uncoupled or coupled by the spin-orbit interaction.

		No spin-orbit		With spin-orbit[a]	
v	j	$^2\Sigma$	$^2\Pi$	$^2\Sigma_{1/2}$	$^2\Pi_{1/2}$
0	0	1.6442	1.6469	1.6284	1.6794
0	2	1.6894	1.6920	1.6735	1.7246
0	4	1.7922	1.7948	1.7764	1.8274
0	6	1.9496	1.9522	1.9337	1.9847
1	0	2.1556	2.1583	2.1397	2.1908
1	2	2.1987	2.2013	2.1828	2.2339
1	4	2.2972	2.2999	2.2814	2.3324
1	6	2.4475	2.4501	2.4317	2.4827
2	0	2.6376	2.6403	2.6218	2.6728

[a]Differences between entries in the two columns to be compared with the atomic fluorine fine structure splitting, $\delta = 0.0501$ eV.
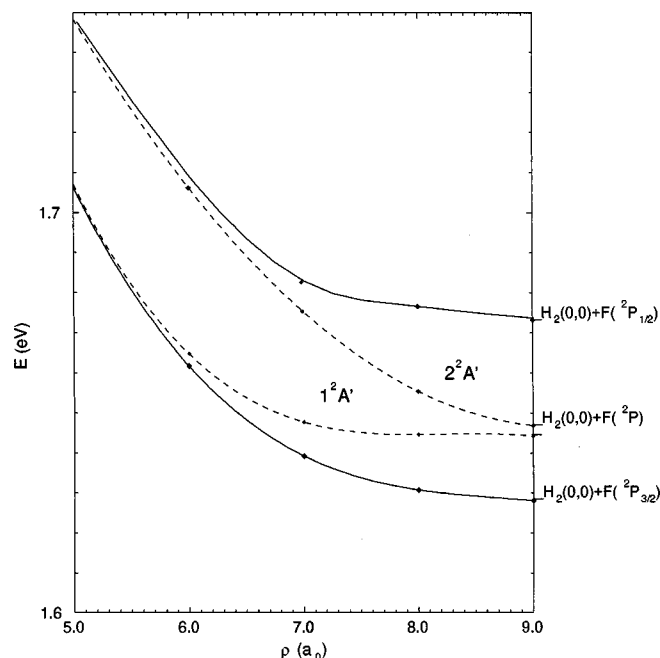
FIG. 5. Curves correlating with the H_2 rotovibrational ground state, as a function of ρ. Dashed curves are obtained from the two uncoupled surfaces. Continuous curves show the effect of the spin-orbit coupling.

The complete diagonalization of the Hamiltonian matrix is seen to give rise to a separation between the eigenvalues on the two surfaces, generating an energetic gap of which the larger is the hyperradius, the closer it gets to the fluorine spin-orbit splitting δ. In particular, curves corresponding to the ground state surface are lower in energy by $\sim 1/3\delta$, those corresponding to the upper surface shift upwards by $\sim 2/3\delta$ (as it must be, being the former surface doubly degenerate). These modifications at long range may be crucial in orienting the reaction dynamics differently than expected considering only a single surface, both advocating a role in the $^2P_{1/2}$ state of fluorine, and influencing the energetics of reaction paths leading over the barrier.

When the ridge line is well above the upper limit of the interesting energy range, the channels can be considered as completely separated. However, the same presence of a ridge enables us to talk about two distinct valleys for reagents and products, so that we can attribute effective potentials to one channel or to another, in the whole region where fine structure effects play a significant role. It is evident that this is an important simplification in order to discuss spin-orbit effect with respect to the entrance channel eigenvalues. The complicated avoided crossing pattern in the manifold of curves reported in Fig. 4 mixes entrance and exit channels and masks the visualization of the effect of the introduction of the upper surface and of the fine structure. Curves correlating to the exit channel (i.e., the rotovibrational levels of the HF molecule) are however unaffected. Therefore, we simplify the discussion focusing our attention only on those eigenvalues which are affected by the couplings (Fig. 5).

Figure 5 is a blow-up of a portion of the relevant eigenvalues correlating to the lowest rotational state of ground state H_2. As expected, the shift between curves induced by inclusion of the spin-orbit effect can be considered substan-

tially quenched already at hyperradius values around $6a_0$. Simple physical principles aid in explaining the decrease of this separation, based on the ratio between energetic distance of the surfaces and the shifting due to spin-orbit coupling on the fluorine atom. At asymptotic values of the hyperradius, where the two surfaces are very close, spin-orbit coupling is most effective, so that fine structure effects sensibly affect adiabatic eigenvalues. In more internal regions, on the other hand, the $\Sigma - \Pi$ separation is large with respect to δ, and spin-orbit interaction less and less manages to significantly couple the surfaces. Therefore, Fig. 5 is an illustration of the previous assertion (Sec. II) that, in the strong interaction regions, the electrostatic forces uncouple nuclear and electronic angular momenta, thus validating the Born–Oppenheimer separation.

IV. CONCLUSIONS

This work has provided a description of the computational implementation of the hyperquantization algorithm. The performances of both symmetric and asymmetric hyperspherical coordinates have been compared, and the former appear typically to be preferred. A comparison with other methods has shown that this new technique is reliable and competitive, especially where the triatomic interaction is strong. In the asymptotic region of reactants and products, the efficiency can presumably be improved by a separate description of the channels and properly dealing with the resulting overcompleteness.

Faster convergence and improvements in both memory and diagonalization time can be achieved by using basis set contraction or similar strategies, for example the diagonalization–truncation[32] procedure, that we are currently implementing and testing. Our technique appears to be more efficient for reactions which are not collinearly dominated, as demonstrated by some test calculations on another potential energy surface for $F+H_2$.[7,33] This aspect, which depends on the nature of the grid, resulting from our discretization procedure based on Hahn polynomials, suggests that future investigation should focus on the use of alternative discrete orthogonal polynomials, such as dual Hahn's and Racah's.

Open-shell and fine structure effects on the $F+H_2$ reactions have also been examined. Inclusion of an upper surface and of the spin-orbit interaction involves little additional effort for this reaction, but its consequences for dynamics can be crucial. This is an illustration of an advantage which is characteristic of our method, which, indexing spatial variables by quantumlike numbers, allows us to introduce physical interactions of the system in the regions of configuration space where these are operative. So, computational effort is not much greater than in the case of the adiabatic treatment on a single surface, in virtue of the limited increase of the overall dimension of the problem. The order of matrices grows by only 15% at the largest considered hyperradius value, $\rho = 9a_0$, and this number decreases for smaller values, where the excited surface sensibly rises.

In conclusion, we believe that the results presented in this work encourage the refinement of the numerical methods involved. They also point out the flexibility of the hyperquantization technique to unify all the symmetries of a sys-

tem within a common framework under the language of angular momentum algebra, and to envisage the possibility of generalizations to more complex systems than triatomic reactions.

APPENDIX: THE DIAGONALIZATION ROUTINES

1. General on Lanczos methods

Both the sparseness and the symmetry properties of our Hamiltonian matrix (see Table III and Ref. 1), make the diagonalization problem ideal for application of a family of algorithms based on Lanczos[34] recurrence formula. This is a procedure of tridiagonalization reduction, where the original matrix, for which we want to obtain a portion of the eigenvalue–eigenvector spectrum, enters in the recursion only through a matrix–vector product term. Thus, the structure of the original matrix is not modified as the computation proceeds. For this reason it is particularly attractive for dealing with very large but sparse and highly structured matrices. The algorithm will be the more efficient the more the routine that generates the matrix–vector product exploits the structure of the problem.

In this Appendix, the discussion focuses on those general features of the diagonalization Lanczos routines that quantitatively influence the efficiency, i.e., storage requirements and CPU time, of our computational technique. The Lanczos procedure can be viewed as a mechanism for generating orthonormal bases for a Krylov subspace and for computing the orthogonal projection of the matrix to be diagonalized onto this particular subspace (see Refs. 35–37 for a detailed review of these methods). The quality of the Krylov subspace and so the convergence rate of the Lanczos recursion is strictly dependent on the starting vector. In practical situations, the Lanczos vectors lose their orthogonality as the recursion proceeds because of finite arithmetics effects. This loss of orthogonality generates a number of spurious eigenvalues within the spectrum. Extensive recent efforts devoted to cope with this problem can be classified into three categories which differ in the strategy used:[35] one of them implements a total and ''blind'' reorthogonalization of each Lanczos vector with respect to each previously generated Lanczos vector; the second one performs reorthogonalization with respect to only those specific vectors which are mainly responsible for the loss of orthogonality; the third

approach simply accepts the loss of orthogonality and then tries to cope directly with the resulting problems.

We have found that algorithms with total reorthogonalization are more efficient and among these we have studied the relevance for the performances of our method of the shifting strategy of Ericsson and Ruhe[38] and of the implicit restarting method of Sorensen and co-workers[39] on the shifted and inverted matrix.

2. Implicit restarting

In the algorithms which use implicit restarting (Arpack package), the dimensions of the Krylov subspace are user-fixed at a reasonably small value (suggested as about twice the number of the desired eigenvalues) in order to minimize the number of reorthogonalization steps and of eigenvectors to be stored. If sufficient accuracy is not achieved the algorithm restarts with a more appropriate vector. When the user-fixed accuracy is reached the algorithm stops.

The convergence rate of the Lanczos methods is strictly dependent from the nature of the eigenvalues. Extremal (at the lower or upper end point of the spectrum) nonclustered eigenvalues converge more quickly than internal and/or clustered ones, and to enhance convergence to a desired portion of the spectrum, a functional transform of the original matrix with a less dense spectrum in the interesting energies range is diagonalized. One of the more commonly used spectral transformations is the ''shift and inversion'' method. To apply the Lanczos recursion to shifted and inverted matrix a linear system solver is needed either with a matrix factorization or with an iterative method. In the former case the original matrix is factorized as the product of a few matrices (often triangular or diagonal matrices) easier to invert than the original one. The factorization routines do not exploit obviously the numerous symmetries of our Hamiltonian matrix (in general only the symmetry with respect to the main diagonal is considered). Moreover the factorized matrix can lose the symmetries and part of the sparseness of the original matrix. For example, at the most basic level, i.e., with no spectral transformation, the Arpack package applies the Lanczos recursion to the matrix to be diagonalized supplying only a matrix–vector product subroutine. Thus if the problem has particular symmetries, as in our case,[1] not all the nonzero elements have to be stored but only those that cannot be obtained by symmetry, and this leads to savings in the memory requirements. However, even with no spectral transform the memory required is about four times smaller, and the sample calculations carried out applying the Arpack package to the shifted and inverted problem show that the inversion allows us to gain an order of magnitude in CPU time. In order to compute the adiabatic eigenvalues in a reasonable time we must apply the Lanczos algorithm to the shifted and inverted matrix.

The Arpack package has some very attractive features: a reverse communication interface that makes it very easy to implement matrix storage and system linear factorization and solver more suitable for the problem to be diagonalized. A parallel version of the package works well with most computer architecture.[40] An interesting feature is the possibility of supplying in a simple way the first starting vector (if no

starting vector is given, a random vector is taken): when the starting vector has a large component along the eigenvector sought, the convergence rate increases rapidly. This property is very important for scattering calculations where a sequence of closely related problems must be solved. A linear combination of the eigenvectors of the previous ρ sectors can be given. Obviously the gain in the convergence rate is not very large when too many eigenvectors are combined. However if not too many eigenvectors are sought for any shift value, only the proper eigenvectors can be combined for each shift to fully exploit this property.

3. Spectral transform

In the Arpack package the shift is user-fixed in the range where the eigenvalues are sought. A different strategy was chosen in the STLM package, based on the algorithm of Ericsson and Ruhe.[38] This package works with total reorthogonalization of the inverted and shifted problem but in this case the shift serves to minimize the dimension of the Krylov subspaces. For each choice of the shift value only the nearest eigenvalues are sought and to obtain convergent eigenvalues only a few Lanczos iterations and Lanczos vectors are needed. In general, a new shift requires a new factorization of the matrix. In the STLM package the number of shifts and consequently the number of iterations for any shift is chosen to optimize the CPU time by monitoring the time required for the factorization and the time for every Lanczos iteration. Alternative choices for spectral transformation are possible[41] but we did not investigate them in this work.

When the shift and inverted problem is solved, the efficiency of the diagonalization is largely dependent on the algorithm chosen to solve the linear system. In particular, the degree of the sparseness of the factorized matrix is affected by the structure of the original matrix and by the factorization procedure. If the factorization is not suited to the problem the memory required can be large. STLM works with an LDL^T factorization, D being a diagonal matrix and L a lower triangular matrix. In the Arpack package the user must supply the factorization and the solver routine. To solve the linear system by iterative algorithms we have used the DSRIS routine of the essl library, and have chosen the conjugate gradient method with an incomplete LU factorization as a preconditioner U being an upper triangular matrix. This choice allows the optimization of the CPU time but not of the memory requirements with respect to other methods and different preconditioners available in this routine. Also the storage method of the matrix can change by many factors the performance. In the STLM package the matrix is given in the skyline form while in the DSRIS subroutine is given in sparse upper storage by rows. The optimization of these two steps with more appropriate algorithms, which take into account the structure of our matrix, is very important for future applications of the hyperquantization algorithm.

From the calculations on sample matrices, we observe that while for the Arpack package the CPU time is approximately proportional to the number of eigenvalues sought, for the STLM package the increase is much slower. From these results we can conclude that the shifting strategy is very important for scattering applications where many hundreds

of eigenvalues are sought. For the reasons discussed above we have used the STLM package in the ''production runs.'' Better performances could probably be obtained by applying the moving shifting strategy of STLM to the implicit restart of the Arpack package. These strategies may be unnecessary using the sequential diagonalization truncation method,[41] which is currently being implemented.

4. Other tests

Finally, we mention that three other routines have been implemented and tested: the L.A.N.Z. package of Patrick and Jones,[42] the L.A.S.O. package of Parlett and Scott[37] (which uses partial reorthogonalization), and the Cullum and Willoughby[43] package (no reorthogonalization). At the present stage of developments, these routines showed no advantages over those employing total reorthogonalization.

The research on Lanczos procedures for computations of eigenvalues and eigenfunctions continues.[44] Although many interesting results have been obtained in the last 20 years, many of the theoretical questions remain unanswered. Many advances were made in this direction and further progress will be made in the near future, as we can judge from the large number of relevant papers already in the literature and from the large number of applications that the sparse matrix problem has in many different disciplines. The efficiency of our hyperquantization algorithm is strictly dependent upon the progress that will be obtained in this particular aspect of computational mathematics.

[1] V. Aquilanti, S. Cavalli, and D. De Fazio, J. Chem. Phys. **109**, 3792 (1998), preceding paper.
[2] (a) V. Aquilanti and S. Cavalli, Few-Body Syst., Suppl. **6**, 573 (1992); (b) V. Aquilanti, S. Cavalli, and G. Grossi, in *Advances in Molecular Vibrations and Collision Dynamics*, edited by J. M. Bowman (JAI, Greenwhich CT, 1993), p. 147; (c) V. Aquilanti, S. Cavalli, C. Coletti, D. De Fazio, and G. Grossi, in *New Methods in Quantum Theory*, edited by C. A. Tsipis, V. S. Popov, D. R. Herschbach, and J. S. Avery (Kluwer, Dordrecht, 1996), p. 233.
[3] D. E. Manolopoulos, J. Chem. Soc., Faraday Trans. **93**, 673 (1997).
[4] R. Steckler, D. G. Truhlar, and B. C. Garrett, J. Chem. Phys. **82**, 5499 (1985).
[5] J. M. Launay and M. Le Dourneuf, Chem. Phys. Lett. **169**, 473 (1990).
[6] G. A. Parker and R. T Pack, J. Chem. Phys. **98**, 6883 (1992).
[7] K. Stark and H. J. Werner, J. Chem. Phys. **104**, 6515 (1996).
[8] M. Gilibert and M. Baer, J. Phys. Chem. **98**, 12822 (1994).
[9] G. D. Billing, L. Yu. Rusin, and M. B. Sevryuk, J. Chem. Phys. **103**, 2482 (1995).
[10] B. Lepetit, M. Le Dourneuf, and J. M. Launay, Chem. Phys. **106**, 103 (1986).
[11] F. Rebentrost and W. A. Lester, Jr., J. Chem. Phys. **67**, 3367 (1977).
[12] C. S. Maierle, G. C. Schatz, M. S. Gordon, P. McCabe, and J. N. L. Connor, J. Chem. Soc., Faraday Trans. **93**, 709 (1997).
[13] Z. Bacic, J. D. Kress, G. A. Parker, and R. T Pack, J. Chem. Phys. **92**, 2344 (1990).
[14] V. Aquilanti, R. Candori, D. Cappelletti, E. Luzzatti, and F. Pirani, Chem. Phys. **145**, 293 (1990).
[15] Notations for hyperangles as in Ref. 1.
[16] U. Fano, Phys. Rev. A **24**, 2402 (1981).
[17] A. Ohsaki and H. Nakamura, Phys. Rep. **187**, 1 (1990).
[18] (a) V. Aquilanti, S. Cavalli, and G. Grossi, Chem. Phys. Lett. **110**, 43 (1984); (b) V. Aquilanti and S. Cavalli, *ibid.* **141**, 309 (1987); (c) V. Aquilanti, S. Cavalli, G. Grossi, V. Pellizzari, M. Rosi, A. Sgamellotti, and F. Tarantelli, *ibid.* **162**, 179 (1989).
[19] (a) V. Aquilanti and G. Grossi, J. Chem. Phys. **73**, 1165 (1980); (b) V. Aquilanti, P. Casavecchia, G. Grossi, and A. Laganà, *ibid.* **73**, 1173 (1980).

[20] V. Aquilanti, S. Cavalli, and D. De Fazio, J. Phys. Chem. **99**, 15694 (1995).

[21] G. Racah, Phys. Rev. **62**, 438 (1942).

[22] D. A. Varshalovich, A. N. Moskalev, and V. K. Khersonskii, *Quantum Theory of Angular Momentum* (World Scientific, Singapore, 1988).

[23] C. C. J. Roothaan and S.-T. Lai, Int. J. Quantum Chem. **63**, 57 (1997).

[24] T. Tamura, Comput. Phys. Commun. **1**, 337 (1970).

[25] (a) J. G. Wills, Comput. Phys. Commun. **2**, 381 (1971); (b) K. Srinivasa Rao and K. Venkatesh, *ibid.* **15**, 227 (1978).

[26] K. Schulten and R. G. Gordon, J. Math. Phys. **16**, 1961 (1975).

[27] K. Schulten and R. G. Gordon, J. Math. Phys. **16**, 1971 (1975).

[28] K. Schulten and R. G. Gordon, Comput. Phys. Commun. **11**, 269 (1976).

[29] A preliminary discussion and several convergence tests for the asymmetric representation, including also Radau parametrization, have been reported previously. Those results are complementary to the ones presented here and that paper should be consulted for further details which would be too long to present here.

[30] S. Cavalli, V. Aquilanti, and M. Monnerville, *Numerical Grid Methods and Their Applications to Schröedinger's Equation*, edited by C. Cerjan (Kluwer, Dordrecht, 1993), p. 25.

[31] (a) J. M. Launay and M. Le Dourneuf, Chem. Phys. Lett. **163**, 178 (1989); (b) J. M. Launay, Theor. Chim. Acta **79**, 183 (1991).

[32] R. W. Heather and J. C. Light, J. Chem. Phys. **79**, 147 (1983).

[33] J. F. Castillo, D. E. Manolopoulos, K. Stark, and H. Werner, J. Chem. Phys. **104**, 6531 (1996).

[34] (a) C. Lanczos, J. Res. Natl. Bur. Stand. Sect. B **45**, 255 (1950); (b) **49**, 33 (1952).

[35] J. K. Cullum and R. A. Willoughby, *Lanczos Algorithms for Large Symmetric Eigenvalue Computations*, Vol. I, *Theory* (Wiley, New York, 1985).

[36] Y. Saad, *Numerical Methods for Large Eigenvalue Problems* (Halsted Wiley, New York, 1992).

[37] B. N. Parlett, *The Symmetric Eigenvalue Problem* (Prentice-Hall, Englewood Cliffs, NJ, 1980).

[38] T. Ericsson and A. Ruhe, Math. Comput. **35**, 1251 (1980).

[39] R. Lehoucq and D. C. Sorensen, Available from netlib@ornl.gov (1994).

[40] K. J. Maschoff and D. C. Sorensen, Proceedings of the Copper Mountain Conference on Iterative Methods, 1996, Vol. I (unpublished).

[41] P. Pendergast, Z. Darakhan, E. F. Hayes, and D. C. Sorensen, J. Comput. Phys. **113**, 201 (1994).

[42] M. T. Jones and M. L. Patrick, Inst. for Comp. Appl. in Scien. and Eng. (ICASE) NASA, Tecn. Rep. 89-67 (1989).

[43] J. K. Cullum and R. A. Willoughby, *Lanczos Algorithms for Large Symmetric Eigenvalue Computations*, Vol. II, *Programs* (Wiley, New York, 1985).

[44] *Book of Abstracts: Workshop on the Use of Iterative Methods for Large-Scale Eigenvalue Problems* May 14–16, 1997 (Argonne National Laboratory, Argonne, IL, 1997).